THE JOURNAL OF PHYSICAL CHEMISTRY B

Article

pubs.acs.org/JPCB

The Entry of HCl through Soluble Surfactants on Sulfuric Acid: Effects of Chain Branching

Daniel K. Burden, Alexis M. Johnson, James M. Krier, and Gilbert M. Nathanson*

Department of Chemistry, University of Wisconsin-Madison, 1101 University Avenue, Madison, Wisconsin 53706, United States

ABSTRACT: Gas−liquid scattering experiments are used to determine how a soluble, branched surfactant (2-ethylbutanol) controls the entry of gaseous HCl molecules into 60 and 68 wt % D_2SO_4 at 213 K. Short-chain alcohols spontaneously segregate to the surfaces of these sulfuric acid solutions, which are representative of aerosol droplets in the lower stratosphere. We find that 2-ethylbutanol enhances HCl entry at low surface coverages, most likely because it provides extra interfacial OH groups that aid HCl dissociation. This enhancement disappears at higher coverages as the alkyl chains crowd each other and block access to the acid. The branched alcohol impedes HCl entry more effectively than its unbranched isomer 1-hexanol, implying that the larger 2-ethybutanol footprint on the surface blocks more HCl molecules from reaching the alcohol-acid interface. This behavior contrasts sharply with gas transport through long-chain monolayers, where branching introduces gaps that allow more facile passage. The experiments suggest that short-chain surfactants with extended footprints may impede transport more effectively than their unbranched isomers.

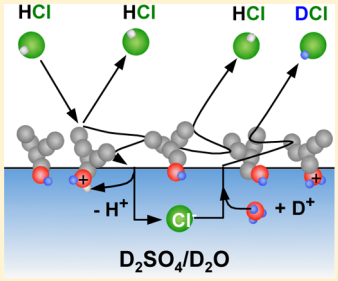

INTRODUCTION

Atmospheric aerosol droplets can behave like nanoscale "chemical reactors" by providing a medium in which airborne organic matter enter and react.[1−3] These droplets range in composition from supercooled sulfuric acid in the midlatitude stratosphere to mixtures of water, salt, and biological and organic species in sea spray just above the ocean surface.[4,5] Organic matter is ubiquitous in the earth's boundary layer but has also been observed in the upper troposphere and even in the lower stratosphere.[6−8] Many of these molecules are amphiphilic and segregate at the droplet surface, where they can significantly alter water transport and the reactivity of nitrogen oxides (such as N_2O_5) and halogen-containing species (such as HCl).[3,9,10] These surfactants include insoluble, long-chain alcohols and carboxylic acids and their soluble, shorter-chain analogues.[6] We explore in this study the effects of chain branching in controlling the entry of HCl into supercooled sulfuric acid by comparing surface films of three short-chain alcohols: the branched 2-ethyl-1-butanol (EtBuOH); its unbranched isomer, 1-hexanol (HexOH); and the shorter chain 1-butanol (BuOH).

Our experiments were motivated by the idea that chain branching might alter gas transport differently in long- and short-chain surfactants. Early studies of monolayer films focused on measurements of water permeation through insoluble fatty acids and alcohols, which revealed that tightly packed, solid-like monolayers of C_{14} to C_{22} primary alcohols provide water permeation resistances r_{mono} of ∼0.5 to 20 s cm^{-1}.[11−15] These values imply that only ∼1 × 10^{-4} to ∼3 × 10^{-6} of the H_2O molecules impinging on the films penetrate through them.[16,17] The permeation resistances increase exponentially with surface density, such that a 4% decrease in the area per molecule increases r_{mono} by two.[14] Branched and bent surfactants sterically hinder tight packing, creating gaps between the chains that reduce their resistance to water permeation to unmeasurable values.[16,18,19] These gaps enable molecules to pass between the chains and to allow "water fingers" to reach through the monolayer.[20]

The remarkable ability of side chains and double bonds to render monolayers more porous has been demonstrated for permeation by other gases. For example, Cosman et al. have shown that methyl side chains in the molecule 3,7,11,15-tetramethyl hexadecanoic acid completely negates the N_2O_5-blocking ability of the straight-chain octadecanoic acid, which reduced N_2O_5 hydrolysis by 17-fold.[21] Similarly, Daumer et al. found that the neutralization of H_2SO_4 with gaseous NH_3 was dramatically reduced by films of 1-hexadecanol, while the extensively branched alcohol 1-adamantanemethanol had no measurable effect.[22] Gilman and Vaida further showed that the uptake of acetic acid into water was strongly hindered by long-chain (C_{18} and C_{30}) alcohols, but the introduction of a double bond to the C_{18} alcohol increased permeation through the monolayer by 13-fold.[23] This behavior was also observed by Stemmler et al., who found that octadecanoic acid monolayers reduced HNO_3 uptake into NaCl-water aerosol particles, while cis-9-octadecenoic acid (with one double bond) had no measurable effect.[24,25]

Short-chain molecules form more loosely packed monolayers[26] that also alter gas transport and reaction, but to a lesser extent. Thornton and Abbatt observed that chains as short as hexanoic acid reduce the reactive uptake of N_2O_5 into salty aerosol particles by a factor of ∼4.[27] The hydrolysis of HNO_3 and NH_3 in water was investigated by Clifford et al., who found

Special Issue: James L. Skinner Festschrift

Received: January 30, 2014
Published: March 12, 2014

   dx.doi.org/10.1021/jp501080g | J. Phys. Chem. B 2014, 118, 7993−8001

that octanol films suppress reaction, whereas butanol had little effect.[28] Donaldson[1,29,30] and Kawasaki[31] and their co-workers have also shown that organic films can enhance uptake if the gas species is more soluble or reactive in the film than in the subphase. Most relevant to the studies here is the report by Caskey et al. that a film of 4-octanol on water inhibits CO_2 transport by 13%, twice as much as a 1-octanol coating at the same surface concentration.[32]

Our own experiments demonstrate that BuOD, HexOD, and 1-pentanoic acid films on deuterated sulfuric acid alter the entry of HCl.[33−36] As depicted in Figure 1a, we found that alkyl

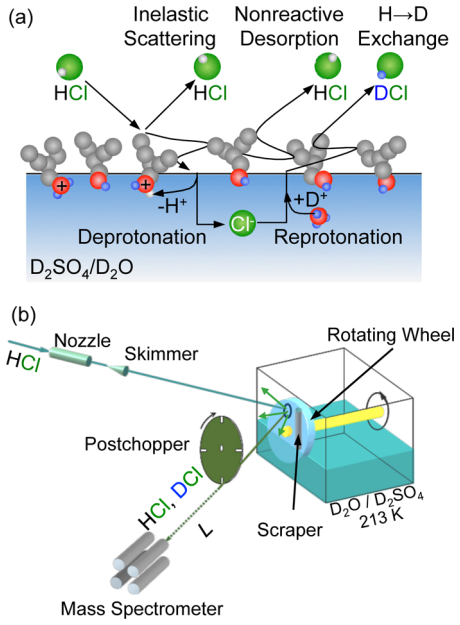

Figure 1. (a) Several possible pathways for an HCl molecule colliding with deuterated sulfuric acid that is partially covered with 2-ethylbutanol. (b) Schematic diagram of the gas−liquid scattering apparatus.

chains block HCl from reaching the surface of the acid, while the alcohol OD groups provide additional interfacial sites for HCl dissociation and thus enhance its entry into the acid. This enhancement channel was not observed for N_2O_5 hydrolysis on BuOD or HexOD films on sulfuric acid and so may be restricted to gaseous acids that are trapped by protonating the OD headgroup.[36] To further explore correlations between molecular structure and gas transport for soluble surfactants, we investigate below the effects of chain branching by comparing HCl uptake through three alcohol monolayers: BuOD [$CH_3(CH_2)_3OD$], HexOD [$CH_3(CH_2)_5OD$], and EtBuOD [$(CH_3CH_2)_2CHCH_2OD$]. Contrary to expectations based on long-chain monolayers, the experiments reveal that the two ethyl branches of EtBuOD are more effective than the single hexyl and butyl chains of HexOD and BuOD in blocking HCl entry into the acid.

Properties of Sulfuric Acid and 1-Butanol, 1-Hexanol, and 2-Ethylbutanol Surfactants. The 60 wt % (10 M) and 68 wt % (12 M) D_2SO_4/D_2O solutions are viscous acid solutions[37] with vapor pressures of 9×10^{-4} and 2×10^{-4} Torr at the acid temperature of 213 K.[38] At both concentrations, D_2SO_4 dissociates and forms mixtures of D_2O, D_3O^+, DSO_4^-, and SO_4^{2-}, with D_2O as the only evaporating species.[39−41] The acidity of these solutions at 213 K may be gauged by their D^+ activities, which in the corresponding (equal mole fraction) 62 and 70 wt % H_2SO_4 solutions are calculated to be 260 and 2600 for H^+.[38] In parallel, the HCl solubility $[Cl^-]/P_{HCl}$, which is governed by the equilibrium $HCl(g) \rightleftharpoons H^+(aq) + Cl^-(aq)$, decreases from 1.0×10^4 to 250 M atm^{-1} in 62 and 70 wt % H_2SO_4 because fewer water molecules are available to be protonated by HCl at the higher acid concentration.[38]

The surfactants BuOH (mp = 188 K), HexOH (mp = 226 K), and EtBuOH (mp = 159 K) dissolve without freezing at 213 K into the 60 and 68 wt % D_2SO_4 solutions at concentrations up to 0.2 M. Each alcohol undergoes protonation to form ROD_2^+ and also reacts slowly at low temperatures to form the sulfate ester, $ROSO_3^-$ and $ROSO_3D$.[42] For ethanol at 298 K, the ratios of EtOH:$EtOH_2^+$ are approximately 2:1 and 1:1 in 62 and 70 wt % H_2SO_4, respectively.[43] We therefore expect the alcohol films to be composed of both ROD and ROD_2^+ and small amounts of $ROSO_3^-$ and $ROSO_3D$.

Figure 2 shows space-filling models of HexOH in the all-trans conformation and EtBuOH in its lowest-energy

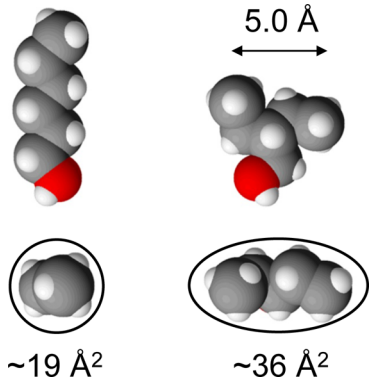

Figure 2. Space-filling models of 1-hexanol (left, all-trans conformation) and 2-ethyl-1-butanol (right) in side and top-down views.

conformation.[44] The most striking difference is the projected area of the alkyl chains: the all-trans chain occupies a minimum area of ~19 Å^2,[45,46] while the branched EtBuOH covers approximately twice this area, with a "footprint" of ~36 Å^2. It is helpful to view 2-ethylbutanol as 2,2-diethylethanol because it terminates in two off-axis ethyl groups that make an asymmetric "Y" shape perpendicular to the surface, with the OH group at the bottom. Based on these surface footprints, a tightly packed monolayer of the bulkier EtBuOH (with a maximum surface concentration c_{surf} of 1/36 Å^2 = 2.8×10^{14} cm^{-2}) is formed at roughly half the density of a single-chain alcohol, which has been observed at densities as high as 5.3×10^{14} cm^{-2}.[14,45]

EXPERIMENTAL PROCEDURE

The 60 and 68 wt % acid solutions were prepared by diluting 98 wt % D_2SO_4 with D_2O and then placing a 60 mL aliquot into the Teflon reservoir pictured in Figure 1b. BuOH, HexOH, or EtBuOH (Sigma-Aldrich) was added to the acid at ~280 K by dropping the alcohol onto the acid with a micropipet. Each alcohol was fully converted into its OD analogue via H→D exchange with the D_2SO_4 solvent, which reduced the deuterium fraction of the solutions by less than 0.3%.

As depicted in Figure 1b, a continuously renewed, vertical liquid film was formed by rotating a 5 cm diameter glass wheel partially submerged in the acid, which is cooled to 213 K.[47] The

dx.doi.org/10.1021/jp501080g | J. Phys. Chem. B 2014, 118, 7993−8001

coated wheel was skimmed by a Teflon scraper, leaving behind a ~0.5 mm thick acid film. The scraped film then passed in front of a 0.7 cm^2 hole in the reservoir, where it was exposed to Ar or HCl for 0.27 s at a typical wheel speed of 0.17 Hz. The time between scraping and exposure to the incident beam was 0.49 s. This replenishment time is sufficient to establish monolayers of each alcohol at the surface of the acid.[34,47,48]

Incident beams of Ar (90 kJ mol^{-1}) and HCl (100 kJ mol^{-1}) were directed at the surface of the acid at an incident angle of 45°, projecting a 0.36 × 0.51 cm^2 beam spot. High-energy HCl and Ar were prepared by expanding 2% mixtures of each gas in H_2 at 1 atm through a glass nozzle with a 0.1 mm diameter aperture. HCl dimer formation was suppressed by heating the nozzle to ~350 K. After scattering or desorbing from the acid, the Ar, HCl, and DCl species were chopped into 40 μs pulses using the postchopper wheel depicted in Figure 1b, and were detected by a doubly differentially pumped mass spectrometer at an exit angle of 45°. Their arrival times t at the mass spectrometer were measured over a 19 cm flight path L and displayed as time-of-flight (TOF) spectra $N(t)$. The translational energies of the molecules and their relative fluxes were computed from $E = 1/2\ m_{gas}(L/t)^2$ and $\int[N(t)/t]dt$.

RESULTS AND ANALYSIS

Surface Tensions and Concentrations. The surface tensions σ of solutions of EtBuOH in 61 and 69 wt % H_2SO_4 at 296 K were measured using the Wilhelmy method[49] and a 1.03 mm diameter Pt pin. These solutions have nearly the same acid mole fractions as the 60 and 68 wt % D_2SO_4 solutions used in the scattering experiments. We used the surface tension measurements to estimate the overall surface excess Γ^{EtBuOH} of neutral, protonated, and esterified EtBuOH using the Gibbs adsorption equation:[50,51]

$$c_{surf}^{EtBuOH} \approx \Gamma^{EtBuOH} \approx \frac{-1}{RT_{liq}}\left(\frac{\partial\sigma}{\partial \ln c_{bulk}^{EtBuOH}}\right)_T \quad (1)$$

where c_{bulk}^{EtBuOH} is the bulk-phase concentration of EtBuOH. The surface excess Γ^{EtBuOH} is likely to be accurate to within ±10% based on an earlier analysis of butanol,[51] while the monolayer surface concentration c_{surf}^{EtBuOH} is equal to Γ^{EtBuOH} to within 1%.[35] Figure 3a,c shows that the surface tensions of the acid solutions decrease steadily with the addition of EtBuOH, HexOH,[35] and BuOH, indicating that these alcohols segregate to the surface of the acid. As anticipated from the more hydrophobic character of six-carbon than four-carbon alcohols, the surface excesses in panels b and d for HexOH and EtBuOH rise more sharply and reach higher asymptotic surface concentrations than for BuOH.

The solid lines in Figure 3 are fits to the surface tension data using a two-parameter Langmuir adsorption isotherm[49]

$$c_{surf} = c_\infty \frac{K_L c_{bulk}}{(1 + K_L c_{bulk})} \quad (2)$$

where c_∞ is the asymptotic surface concentration and K_L gauges the alcohol's propensity for segregation. We use eq 2 to provide an analytic fit for c_{surf} over the range of data in Figure 3.

Table 1 shows that the K_L values for HexOH and EtBuOH are similar and roughly 7 times greater than for BuOD, as mirrored in their steeper rise in Figure 3. Precise comparisons among the c_∞ values are difficult because of the lack of data at high surface coverages. Instead, we compare surface concentrations fit by eq 2 at the highest bulk-phase concentrations used in the scattering experiments: 0.1 M for HexOH and EtBuOH and 0.2 M for BuOH. These c_{surf} values are 2.2, 2.5, and 2.9 × 10^{14} cm^{-2} for BuOH, EtBuOH, and HexOH in 61 wt % H_2SO_4 and 2.0, 2.3, and 2.6 × 10^{14} cm^{-2} in 69 wt % acid. At

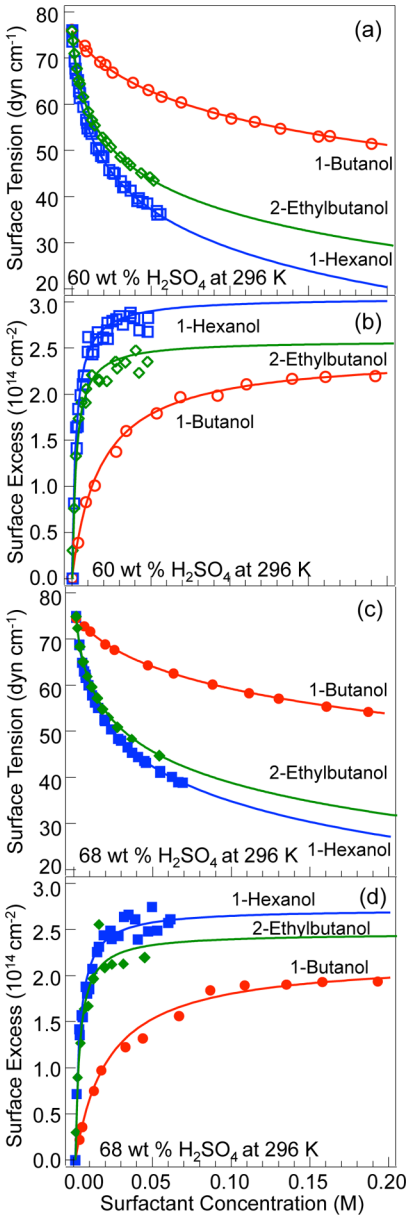

Figure 3. Surface tensions and surface excesses (eq 1) for 61 and 69 wt % H_2SO_4 solutions of BuOH (red), HexOH (blue) and EtBuOH (green) at 296 K. The solid lines are fits to eq 2.

Table 1. Langmuir Fitting Parameters for Alcohol Films on Sulfuric Acid at 296 K[a]

	61 wt % H_2SO_4		69 wt % H_2SO_4	
surfactant	c_∞ (10^{14} cm^{-1})	K_L(M^{-1})	c_∞ (10^{14} cm^{-1})	K_L (M^{-1})
1-butanol	2.43 ± 0.06	55 ± 5	2.17 ± 0.04	50 ± 3
1-hexanol	3.0 ± 0.1	390 ± 50	2.69 ± 0.04	360 ± 20
2-ethylbutanol	2.6 ± 0.1	410 ± 60	2.4 ± 0.1	380 ± 50

[a]The error bars represent 95% confidence intervals of the least-squares fits to the surface tension data in Figure 3a,c using the relation $\gamma - \gamma(\text{bare acid}) = -RTc_\infty \ln(1+ K_L c_{bulk})$.

dx.doi.org/10.1021/jp501080g | J. Phys. Chem. B 2014, 118, 7993−8001

these coverages, the EtBuOH molecules nominally occupy ~85% of the surface area, while BuOH and HexOH occupy ~40% and ~50% of the surface in their all trans-conformations. Preliminary measurements indicate that BuOH and HexOH surface concentration are 5−10% higher at 250 K than at 296 K, which suggest that they may be 10−20% higher at 213 K. Because of these differences, we focus on trends rather than on the absolute values of the measurements.

Surface vibrational sum frequency generation (VSFG) experiments[52] and molecular dynamics (MD) simulations[53−55] provide microscopic views of the packing of BuOH and HexOH on water and on sulfuric acid. VSFG experiments by Van Loon et al. indicate that BuOH is partially disordered on 59.5 wt % H_2SO_4 at 0.052 M BuOH, but more of the molecules adopt all-trans conformations at higher bulk concentrations and perhaps forms islands on the surface.[52] In parallel, MD simulations by Sakaguchi and Morita indicate that neutral BuOH segregates to the outermost layer of 58 wt % H_2SO_4 and that $BuOH_2^+$ lies just below, each adopting a variety of conformations and orientations that roughen the bare surface.[55] HexOH, with two more CH_2 units than BuOH, is observed by VSFG to possess more gauche conformations. These different configurations potentially orient some of the hexyl chains to shadow and block the surface, as inferred later in the Discussion.

Hyperthermal Argon Scattering from Surfactant Films on Sulfuric Acid. High-energy Ar atom scattering can be used to detect surfactant molecules in vacuum because their alkyl chains alter the mass and roughness of the surface.[47] Figure 4a shows TOF spectra of 90 kJ mol^{-1} Ar atoms scattered from 0 to 40 mM EtBuOD solutions in 60 wt % D_2SO_4. The spectra are composed of a sharp inelastic scattering (IS) component at early arrival times and a broad thermal desorption (TD) peak at later arrival times. The TD component is fit well by a Maxwell−Boltzmann distribution at the 213 K temperature of the acid, indicating that the Ar atoms in this channel have completely thermalized before desorbing.

The presence of surfactants at the interface significantly alters collisions of Ar with the surface, as shown in Figure 4a. As the EtBuOD concentration is increased, the intensity of the IS component decreases, and the peak shifts to later arrival times. Concurrently, the TD channel increases in intensity. These changes imply that the loosely packed surfactant molecules redirect incident Ar atoms toward other chains, promoting multiple collisions and greater energy loss.

The shift in arrival times in the IS channel (dashed arrow in Figure 4a) may be used to calculate the fractional energy lost by inelastically scattered Ar atoms from surfactant-coated solutions, equal to $[\langle E_{IS}\rangle_{pure} - \langle E_{IS}\rangle_{surf}]/\langle E_{IS}\rangle_{pure}$. These shifts are shown for BuOD, HexOD, and EtBuOD in 60 and 68 wt % D_2SO_4 in Figure 4b,c. The changes in $\langle E_{IS}\rangle$ match the trends in the surface excess curves in Figure 3, suggesting that the vertical films made in vacuum at 213 K mimic those prepared horizontally at 296 K on the benchtop. Figure 5 directly compares the fractional energy transfers (Figure 4b,c) with the surface excesses (Figure 3b,d). It shows that the BuOD and HexOD data fall roughly on the same line but that Ar atoms transfer less energy to the EtBuOD film. This data implies that the branched alcohol presents a stiffer monolayer than do the straight-chain butyl and hexyl alcohols. In particular, the restricted torsional motions of the terminal ethyl branches in EtBuOD may effectively create a more rigid and crowded

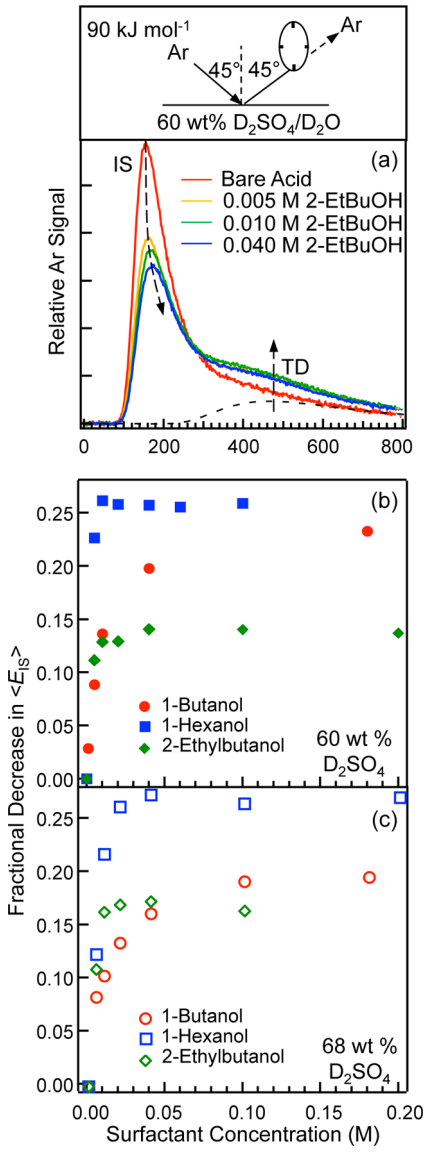

Figure 4. (a) TOF spectra of 90 kJ mol^{-1} Ar atoms scattering from solutions containing 2-ethylbutanol at 213 K. Panels b and c show the fractional decrease in energy in the inelastic scattering channel, $[\langle E_{IS}\rangle_{pure} - \langle E_{IS}\rangle]/\langle E_{IS}\rangle_{pure}$, for BuOD, HexOD, and EtBuOD for (b) 60 wt % and (c) 68 wt % D_2SO_4.

monolayer of short ethyl chains and thereby reduce the number of modes that can absorb energy from the Ar atom.[56,57]

H→D Exchange in Collisions of HCl with Surfactant Films on Sulfuric Acid. Figure 6a shows HCl and DCl TOF spectra following collisions of high energy (E_{inc} = 100 kJ mol^{-1}) HCl molecules with a 5 mM solution of 2-ethylbutanol in 60 wt % D_2SO_4 at 213 K. Like the Ar TOF spectrum, the HCl spectrum is composed of a sharp inelastic-scattering (IS) peak at short arrival times and a broad thermal-desorption (TD) component at later arrival times. This TD component is fit well by a Maxwell−Boltzmann distribution at 213 K, indicating that the evaporating HCl molecules thermally equilibrate at the surface but escape before reacting.

The DCl TOF spectrum pictured just below the HCl curve in Figure 6a arises from HCl molecules that have undergone HCl → DCl exchange before desorbing. This exchange likely occurs through pathways such as those illustrated in Figure 1a,

dx.doi.org/10.1021/jp501080g | J. Phys. Chem. B 2014, 118, 7993−8001

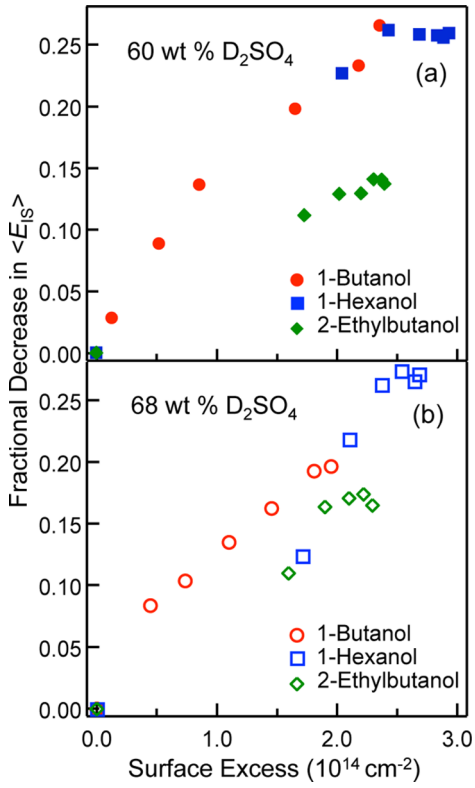

Figure 5. Plots of $[\langle E_{IS}\rangle_{pure} - \langle E_{IS}\rangle]/\langle E_{IS}\rangle_{pure}$, obtained from Figure 4, versus the surface excess of each surfactant, obtained from Figure 3. The fractional energy transfers are smaller for EtBuOD than for HexOD or BuOD.

in which HCl dissociates into Cl^- and H^+ and Cl^- then combines with solvent D^+, dissociating and recombining many times before desorbing as DCl. The TOF spectrum is well fit by a Maxwell–Boltzmann distribution at 213 K and shows no evidence for a direct reaction between HCl and surface species to produce DCl that bypasses HCl thermalization. The HCl and DCl thermal-desorption signals can be used to calculate the probability f_{exch} that thermally equilibrated HCl molecules undergo exchange with the deuterated acid:

$$f_{exch} = \frac{I_{TD}^{DCl}}{I_{TD}^{DCl} + I_{TD}^{HCl}} \quad (3)$$

where I_{TD}^{DCl} and I_{TD}^{HCl} are the integrated fluxes of thermally desorbing DCl and HCl molecules. In this calculation, we assume that DCl and HCl molecules evaporate with equal angular distributions (likely cosine),[58] such that the ratio of the TD fluxes measured at the 45° exit angle is equal to the ratio of the angle-integrated fluxes.

Our previous studies of low and high incident energy HCl scattering show that f_{exch} is independent of HCl collision energy, implying that only thermally equilibrated HCl molecules react with the acid.[33,35,59] Residence time measurements further indicate that HCl molecules that thermalize but do not react must desorb faster than we can measure (less than 1 μs), implying that these unreacted HCl molecules dissipate their kinetic energy through multiple collisions but desorb before penetrating to the alcohol-acid interface. This picture is verified by MD simulations of collisions of H_2O with butanol-coated water[60] and sulfuric acid,[55] which yield 10 ps residence times and several Angstrom penetration depths for these

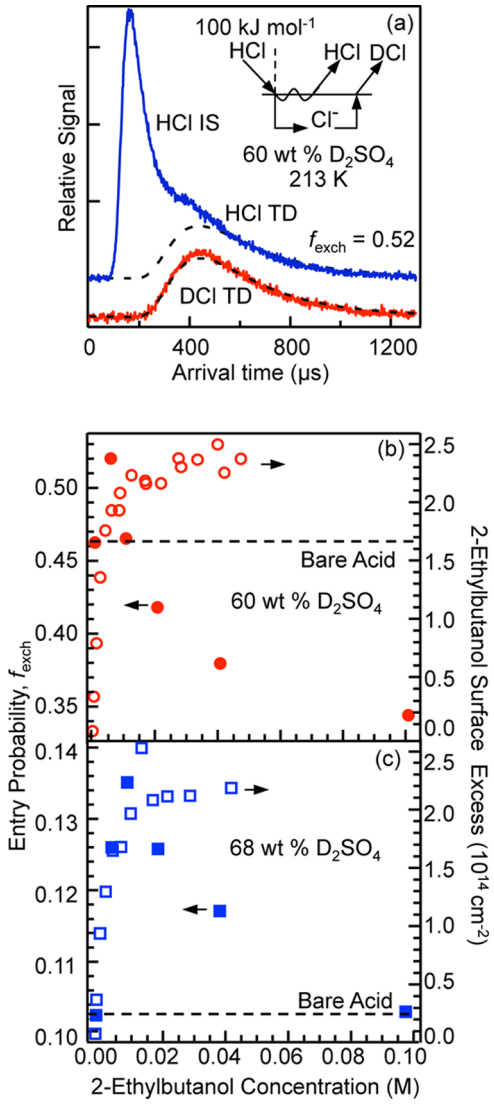

Figure 6. (a) TOF spectra of HCl (blue) and DCl (red) from a 0.005 M solution of EtBuOD in 60 wt % D_2SO_4 following collisions of HCl molecules with E_{inc} = 100 kJ mol^{-1}. The dashed lines are Maxwell–Boltzmann distributions at the 213 K temperature of the acid. Panels b and c show the HCl entry probability (solid symbols) as a function of EtBuOD concentration in (b) 60 and (c) 68 wt % D_2SO_4. The open symbols are EtBuOH surface excesses from Figure 3.

trapping-desorption events. In contrast, HCl molecules that undergo HCl → DCl exchange enter the acid and dissolve for long times (130 μs average residence time in 60 wt % D_2SO_4 at 213 K).[33,59,61] These HCl/Cl^-/DCl species diffuse through the liquid over a depth of approximately $(D\tau/2)^{1/2} \approx 200$ Å for $D = 4 \times 10^{-8}$ cm^2 s^{-1} and $\tau = 130$ μs.[62]

The different time and depth scales imply that I_{TD}^{DCl} in eq 3 equals the flux of HCl molecules that enter the acid solution and emerge as H → D exchanged DCl, while I_{TD}^{HCl} equals the flux of HCl molecules that dissipate their excess energy but desorb before entering the acid. As the incident energy approaches the average thermal energy of $2RT$, nearly all impinging HCl molecules dissipate their translational energy upon collision.[33,35,59] At these thermal collision energies, f_{exch} becomes equal to the probability that impinging HCl molecules enter into the surfactant-coated solution. We note that the residence time measurements do not indicate whether HCl

dx.doi.org/10.1021/jp501080g | J. Phys. Chem. B 2014, 118, 7993–8001

dissociates into H^+ and Cl^- in the interfacial region and then enters as ions or whether HCl passes through the interfacial region as an intact molecule and then dissociates upon more complete solvation. MD simulations, however, suggest that dissociation into an H^+ Cl^- ion pair occurs within the outermost 1−2 monolayers of liquid water,[63,64] methanol clusters,[65] and liquid glycerol.[66]

Figure 6b,c shows f_{exch} (solid symbols) as a function of bulk EtBuOD concentration in 60 and 68 wt % D_2SO_4. Each value is the average of two measurements using the same acid solution, with typical differences of less than 0.01. The surface coverages (open symbols) from Figure 3 are plotted on the right axis. For bare 60 wt % D_2SO_4, f_{exch} is measured to be 0.46, implying that 46% of the thermalized HCl molecules dissociate and enter into solution before desorbing as DCl. Upon addition of EtBuOD to 60 wt % D_2SO_4 at 0.005 M ($c_{surf} \approx 1.7 \times 10^{14}$ cm^{-2}), the HCl entry probability increases to 0.52. Thus, EtBuOH enhances the entry of HCl at low concentrations. HCl uptake then drops steadily below the bare acid value to 0.35 when the EtBuOD concentration reaches 0.1 M ($c_{surf} \sim 2.3 \times 10^{14}$ cm^{-2}). This net blocking was not observed for BuOD or HexOD.[33,34] Figure 6c reveals that HCl entry into 68 wt % D_2SO_4 increases from 0.10 on bare acid to ∼0.13 and then drops back to the bare acid value at 0.1 M EtBuOD, but does not fall below the bare acid value. These trends are discussed below and compared to f_{exch} values for BuOD and HexOD, which have been reported before.[33−35] The BuOD values were measured again for this comparison.

DISCUSSION

Alkyl Chain Blocking and OD Head Group Protonation. The probabilities for HCl entry through films of BuOD, HexOD, and EtBuOD are collected together in Figure 7 by plotting $\Delta f_{exch} = f_{exch} - f_{exch}(bare)$ against c_{surf}/c^*, where $f_{exch}(bare)$ is the HCl → DCl exchange fraction for the bare acid and c_{surf} is calculated using eq 2 and Table 1. The normalization constant c^* is set equal to 5×10^{14} cm^{-2}, near the maximum packing of single alkyl chains, which limits the ratio c_{surf}/c^* to ∼1 for BuOH and HexOH and to ∼0.6 for EtBuOH. By choosing the same c* for all three alcohols, Figure 7 is constructed to reflect trends in f_{exch} per molecule rather than per alkyl chain (one chain for BuOH and HexOH and two branches for EtBuOH).

Figure 7 indicates that the HCl entry probability increases steadily for BuOD but bends over for HexOD and EtBuOD at higher surface concentration. Above $c_{surf}/c^* = 0.3$, the HCl entry probability decreases in the order BuOD > HexOD > EtBuOD at both acid concentrations and highlights the ability of the branched, bulky alcohol to block HCl uptake better than its straight-chain analogue. Only in the case of EtBuOD on 60 wt % acid does the surface film lower the HCl entry probability below the bare acid value, from 0.46 to 0.35.

The data in Figure 7 can be analyzed quantitatively by applying a model developed for HCl transport through films of HexOD, 1-pentanoic acid, and their mixtures.[35] These studies imply that HCl entry into sulfuric acid coated with short-chain surfactants is controlled by two competing effects brought about by the hydrophobic alkyl chains, which hinder HCl entry, and by the hydrophilic OD headgroups, which provide extra OD sites for HCl hydrogen bonding and dissociation. We assume that incoming HCl molecules dissipate their excess energy via multiple collisions[55,60] with $D_2O/DSO_4^-/D_3O^+/SO_4^{2-}$ species at the surface of the bare acid or with the alkyl

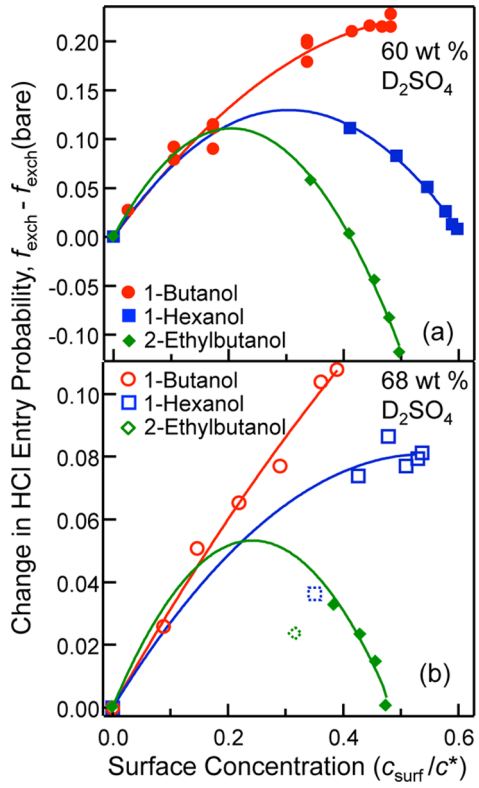

Figure 7. Changes in f_{exch} (HCl entry probability) versus scaled surface concentration for solutions containing BuOD, HexOD, and EtBuOD in (a) 60 wt % and (b) 68 wt % D_2SO_4 at 213 K. The EtBuOD surface concentrations and f_{exch} values are from Figures 3 and 6, the HexOD values are from ref 35, and the BuOD values were remeasured from ref 33 for this study. The solid lines in each panel are fits using eq 4. The two dashed points in (b) were not included in these fits. Their low values may be due to incorrect pipetting or incomplete mixing of the small aliquots of each alcohol added to the acid.

groups of the $ROD/ROD_2^+/ROSO_3^-$ species. The adsorbed HCl molecules then move through fluctuating spaces between the chains with a probability $p_{transport}$, while those that do not fully penetrate instead desorb back into the gas phase. HCl molecules that reach the headgroup-sulfuric acid interface dissociate by protonating ROD or D_2O, followed by Cl^- and H^+/D^+ diffusion into the acid, with a probability $p_{dissociate}$. The overall HCl entry probability, equal to f_{exch}, is given by the product of these probabilities:

$$f_{exch}(\text{surfactant}) = p_{transport} \times p_{dissociate} \quad (4a)$$

$$= \left[1 - a\frac{c_{surf}}{c^*}\right] \times \left[f_{exch}(\text{bare}) + b\frac{c_{surf}}{c^*}\right] \quad (4b)$$

The propensity for HCl transport through the film, $p_{transport} = 1 - a(c_{surf}/c^*)$, is assumed to decrease linearly with surface ROD concentration, weighted by the constant a that measures the efficacy of the alkyl chains to block HCl access to the acid. The HCl dissociation probability, $p_{dissociate} = f_{exch}(bare) + b(c_{surf}/c^*)$, is assumed to increase linearly with surface ROD concentration. The constant b measures the net OD enhancement, that is, the difference in HCl entry probability due to the addition of OD protonation sites provided by interfacial ROD molecules and the disappearance of any D_2O protonation sites that might be tied up or displaced by the surfactant. Both constants a and b are found to be positive for all three alcohols.

dx.doi.org/10.1021/jp501080g | J. Phys. Chem. B 2014, 118, 7993−8001

Table 2. Blocking and Enhancement Parameters for HCl Entry into Sulfuric Acid[a]

	60 wt % D_2SO_4 (f_{exch}(bare) = 0.46)		68 wt % D_2SO_4 (f_{exch}(bare) = 0.10)	
surfactant	blocking parameter (a)	enhancement parameter (b)	blocking parameter (a)	enhancement parameter (b)
1-butanol	0.65 ± 0.08	1.1 ± 0.1	0.34 ± 0.04	0.37 ± 0.06
1-hexanol	1.05 ± 0.05	1.34 ± 0.07	0.80 ± 0.03	0.36 ± 0.08
2-ethylbutanol	1.48 ± 0.06	1.8 ± 0.1	1.5 ± 0.1	0.59 ± 0.09

[a]The error bars represent ±95% confidence intervals of the least-squares fit of eq 4 and include the uncertainties in Table 1.

Comparison of EtBuOD, HexOD, and BuOD. The a and b parameters are collected in Table 2. They fit most of the data in Figure 7 well, but no single data set stringently tests the model by both increasing and then bending over. In particular, the nearly linear trends for BuOD imply small blocking parameters that are difficult to quantify, while the parameters for HexOD on the two subphases are inferred from opposite upward and downward parts of the curve. Two trends in Table 2 appear to be robust. First, the enhancement parameter b is nearly three times smaller for all three alcohol films on 68 wt % D_2SO_4 than on 60 wt % D_2SO_4. This trend most likely arises because of the greater fraction of ROD_2^+ and D_3O^+ at the higher acid concentration and because the alcohol and water OD groups may be more tied up through strong hydrogen bonding interactions with interfacial D_3O^+ and DSO_4^- ions. This reduced fraction of available OD groups is likely the same reason why the HCl entry probability into the bare acid is smaller at higher acid concentrations.[67] We also note that the enhancement parameters are larger for the branched alcohol than for the unbranched ones. This trend may be an artifact of the model or reflect the potentially higher basicity of the longer chain and branched alcohols.[68,69]

Second, the sharp downward curvatures in Figure 7 and inferred blocking parameters a in Table 2 increase in the order BuOD < HexOD < EtBuOD. The greater blocking power of HexOD over BuOD implies that HCl molecules are impeded more by the longer alkyl chain because they must follow a more tortuous path between the chains. HexOD may also be more effective than BuOD because it can adopt more bent conformations that make the chain cover a larger surface area. The similar blocking parameters for EtBuOD on 60 and 68 wt % D_2SO_4, where data is available in the downward part of both curves, suggests that the branched alcohol molecules pack in similar ways on the two acid subphases at the same surface coverage, despite the greater fraction of $EtBuOD_2^+$ at the higher acid concentration. This similarity may arise because the chains still crowd each other even if the $EtBuOD_2^+$ species are shifted deeper into the liquid than the neutral alcohol.[55,70]

The model also predicts that the blocking parameter for EtBuOD is 50 to 100% greater than for HexOD, and Figure 7 indicates that only the branched alcohol is capable of lowering the HCl entry probability below the bare acid value. Although these results would not be predicted from studies of long-chain surfactants, as reviewed in the Introduction, they seem to be a natural consequence of the larger footprint of EtBuOD, which at 0.1 M has a surface density of 2.3×10^{14} cm^{-2} and occupies roughly 85% of the surface at 296 K and even higher values at lower temperatures. This comparison implies that the crowding among the off-axis ethyl groups creates even more constrained paths for HCl diffusion than do the bent conformations available to the single six-carbon chain in HexOD. We hope that MD simulations of water transport through normal alcohols[20,55,60] may be extended to provide more dynamical insights into the time scales and pathways for gas transport through branched alcohols, complemented by experimental measurements of water and HCl uptake over a range of temperatures.

Chain Branching in Soluble versus Insoluble Surfactants. We conclude by noting that the opposite ways in which chain branching alters gas transport through short- and long-chain surfactants may be explained in part by their different packing densities. A long-chain, insoluble surfactant can pack so tightly (up to 5.3×10^{14} cm^{-2} or less than 20 Å^2 molecule^{-1}) that branches introduced into the alkyl chain actually push the individual chains apart,[45] creating gaps for gas molecules to traverse the film. For soluble surfactants such as EtBuOH, HexOH, and BuOH, the alkyl chains are too short to allow solid-like packing (packings observed here were no greater than 2.7×10^{14} cm^{-2} or 34 Å^2 molecule^{-1} for HexOD) because further squeezing causes the surface molecules to dissolve into the bulk subphase. Thus, the addition of branching in EtBuOD monolayers does not introduce "defects" into the porous monolayer, but instead doubles the surface "footprint" of each molecule by effectively splitting the main alkyl chain into two terminal ethyl branches. The result is a less flexible structure (with fewer possible conformations and motions) that covers twice as much of the acid surface and blocks more pathways between the chains when compared to films of the unbranched BuOD and HexOD. It will be intriguing to learn if this branching also impedes gas transport more effectively on less acidic subphases such as seawater containing both salts and organic matter.[5]

AUTHOR INFORMATION

Corresponding Author

*E-mail: nathanson@chem.wisc.edu.

Notes

The authors declare no competing financial interest.

ACKNOWLEDGMENTS

We are grateful to the Air Force Office of Scientific Research for funding this study and to Betsy Solom and Ryan Connelly for assistance with the surface tension measurements. We also thank Tim Bertram, Vicki Grassian, and Kim Prather for insightful discussions about surfactant coatings.

REFERENCES

(1) Donaldson, D. J.; Vaida, V. The Influence of Organic Films at the Air–Aqueous Boundary on Atmospheric Processes. *Chem. Rev.* **2006**, *106*, 1445–1461.

(2) Kolb, C. E.; Cox, R. A.; Abbatt, J. P. D.; Ammann, M.; Davis, E. J.; Donaldson, D. J.; Garrett, B. C.; George, C.; Griffiths, P. T.; Hansen, D. R.; Kulmala, M.; McFiggans, G.; Poschl, U.; Riipinen, I.; Rossi, M. J.; Ruchid, Y.; Wagner, P. E.; Winkler, P. M.; Worsnop, D. R.; O'Dowd, C. D. O. An Overview of Current Issues in the Uptake of Atmospheric Trace Gases by Aerosols and Clouds. *Atmos. Chem. Phys.* **2010**, *10*, 10561–10605.

(3) Abbatt, J. P. D.; Lee, A. K. Y.; Thornton, J. A. Quantifying Trace Gas Uptake to Tropospheric Aerosol: Recent Advances and Remaining Challenges. *Chem. Soc. Rev.* **2012**, *41*.
(4) Carslaw, K. S.; Peter, T.; Clegg, S. L. Modeling the Composition of Liquid Stratospheric Aerosols. *Rev. Geophys.* **1997**, *35*, 125−154.
(5) Prather, K. A.; Bertram, T. H.; Grassian, V. H.; Deane, G. B. Bringing the Ocean into the Laboratory to Probe the Chemical Complexity of Sea Spray Aerosol. *Proc. Natl. Acad. Sci. U. S. A.* **2013**, *110*, 7550−7555.
(6) Gill, P. S.; Graedel, T. E.; Weschler, C. J. Organic Films on Atmospheric Aerosol Particles, Fog Droplets, Cloud Droplets, Raindrops, and Snowflakes. *Rev. Geophys. Space Phys.* **1983**, *21*, 903−920.
(7) Murphy, D. M.; Thomson, D. S.; Mahoney, T. M. J. In Situ Measurements of Organics, Meteoritic Material, Mercury, and Other Elements in Aerosols at 5 to 19 Kilometers. *Science* **1998**, *282*, 1664−1669.
(8) Schmale, J.; Schneider, J.; Jurkat, T.; Voigt, C.; Kalesse, H.; Rautenhaus, M.; Lichtenstern, M.; Schlager, H.; Ancellet, G.; Arnold, F.; Gerding, M.; Mattis, I.; Wendisch, M.; Borrmann, S. Aerosol Layers from the 2008 Eruptions of Mount Okmok and Mount Kasatochi: In Situ Upper Troposphere and Lower Stratosphere Measurements of Sulfate and Organics over Europe. *J. Geophys. Res.* **2010**, *115*, D00L07.
(9) Hanson, D. R.; Lovejoy, E. R. Heterogeneous Reactions in Liquid Sulfuric Acid: HOCl + HCl as a Model System. *J. Phys. Chem.* **1996**, *100*, 6397−6405.
(10) Talukdar, R. K.; Burkholder, J. B.; Roberts, J. M.; Portmann, R. W.; Ravishankara, A. R. Heterogeneous Interaction of N_2O_5 with HCl Doped H_2SO_4 under Stratospheric Conditions: $ClNO_2$ and Cl_2 Yields. *J. Phys. Chem. A* **2012**, *116*, 6003−6014.
(11) Langmuir, I.; Shaefer, V. J. Rates of Evaporation of Water through Compressed Monolayers on Water. *J. Franklin Inst.* **1943**, *235*, 119−162.
(12) Archer, R. J.; La Mer, V. K. The Rate of Evaporation of Water through Fatty Acid Monolayers. *J. Phys. Chem.* **1955**, *59*, 200−208.
(13) La Mer, V. K.; Healy, T. W.; Aylmore, L. A. G. The Transport of Water through Monolayers of Long-Chain n-Paraffinic Alcohols. *J. Colloid Sci.* **1964**, *19*, 673−684.
(14) Barnes, G. T. Permeation through Monolayers. *Colloid Surf., A: Physicochem. Eng. Aspects* **1997**, *126*, 149−158.
(15) For recent studies, see Davies, J. F.; Miles, R. E. H.; Haddrell, A. E.; Reid, J. P. Influence of Organic Films on the Evaporation and Condensation of Water in Aerosol. *Proc. Natl. Acad. Sci. U. S. A.* **2013**, *110*, 8807−8812.
(16) Barnes, G. T. The Effects of Monolayers on the Evaporation of Liquids. *Adv. Colloid Interface Sci.* **1986**, *25*, 89−200.
(17) The permeation probabilities are computed from $4/(\langle v\rangle\, r_{mono})$, where $\langle v\rangle$ is the thermal H_2O thermal velocity $(8RT/\pi m)^{1/2}$. See ref 16.
(18) Rosano, H. L.; La Mer, V. K. The Rate of Evaporation of Water through Monolayers of Esters, Acids and Alcohols. *J. Phys. Chem.* **1956**, *60*, 348−353.
(19) Barnes, G. T. The Potential for Monolayers to Reduce the Evaporation of Water from Large Water Storages. *Agric. Water Manag.* **2008**, *95*, 339−353.
(20) Sakaguchi, S.; Morita, A. Mass Accommodation Mechanism of Water through Monolayer Films at Water/Vapor Interface. *J. Chem. Phys.* **2012**, *137*, 064701.
(21) Cosman, L. M.; Knopf, D. A.; Bertram, A. K. N_2O_5 Reactive Uptake on Aqueous Sulfuric Acid Solutions Coated with Branched and Straight-Chain Insoluble Organic Surfactants. *J. Phys. Chem. A* **2008**, *112*, 2386−2396.
(22) Daumer, B.; Niessner, R.; Klockow, D. Laboratory Studies of the Influence of Thin Organic Films on the Neutralization Reaction of H_2SO_4 Aerosol with Ammonia. *J. Aerosol. Sci.* **1992**, *23*, 315−325.
(23) Gilman, J. B.; Vaida, V. Permeability of Acetic Acid through Organic Films at the Air−Aqueous Interface. *J. Phys. Chem. A* **2006**, *110*, 7581−7587.
(24) Stemmler, K.; Vlasenko, A.; Guimbaud, C.; Ammann, M. The Effect of Fatty Acid Surfactants on the Uptake of Nitric Acid to Deliquesced NaCl Aerosol. *Atmos. Chem. Phys.* **2008**, *8*, 5127−5141.
(25) See also McNeill, V. F.; Wolfe, G. M.; Thornton, J. A. The Oxidation of Oleate in Submicron Aqueous Salt Aerosols: Evidence of a Surface Process. *J. Phys. Chem. A* **2007**, 111−1083 This study shows that sodium sulfate-water aerosol particles containing containing sodium oleate significantly reduce N_2O_5 uptake even though oleate contains one double bond. This result is discussed further in ref 21..
(26) Can, S. Z.; Mago, D. D.; Esesnturk, O.; Walker, R. A. Balancing Hydrophobic and Hydrophilic Forces at the Water/Vapor Interface: Surface Structure of Soluble Alcohol Monolayers. *J. Phys. Chem. C* **2007**, *111*, 8739−8748.
(27) Thornton, J. A.; Abbatt, J. P. D. N_2O_5 Reaction on Submicron Sea Salt Aerosol: Kinetics, Products, and the Effect of Surface Active Organics. *J. Phys. Chem. A* **2005**, *109*, 10004−10012.
(28) Clifford, D.; Bartels-Rausch, T.; Donaldson, D. J. Suppression of Aqueous Surface Hydrolysis by Monolayers of Short Chain Organic Amphiphiles. *Phys. Chem. Chem. Phys.* **2007**, *9*, 1362−1369.
(29) Henderson, E. A.; Donaldson, D. J. Influence of Organic Coatings on Pyrene Ozonolysis at the Air−Aqueous Interface. *J. Phys. Chem. A* **2011**, *116*, 423−429.
(30) Reeser, D. I.; Kwamena, N.-O. A.; Donaldson, D. J. Effect of Organic Coatings on Gas-Phase Nitrogen Dioxide Production from Aqueous Nitrate Photolysis. *J. Phys. Chem. C* **2013**, *117*, 22260−22267.
(31) Hayase, S.; Yabushita, A.; Kawasaki, M.; Enami, S.; Hoffmann, M. R.; Colussi, A. J. Weak Acids Enhance Halogen Activation on Atmospheric Water's Surfaces. *J. Phys. Chem. A* **2011**, *115*, 4935−4940.
(32) Caskey, J. A.; Michelse, D. L.; To, Y. P. Effect of Surfactant Hydrophilic Group on Gas Absorption Rates. *J. Colloid Interface Sci.* **1973**, *42*, 62−69.
(33) Lawrence, J. R.; Glass, S. V.; Park, S. C.; Nathanson, G. M. Surfactant Control of Gas Uptake: Effect of Butanol Films on HCl and HBr Entry into Supercooled Sulfuric Acid. *J. Phys. Chem. A* **2005**, *109*, 7458−7465.
(34) Glass, S. V.; Park, S. C.; Nathanson, G. M. Evaporation of Water and Uptake of HCl and HBr through Hexanol Films at the Surface of Supercooled Sulfuric Acid. *J. Phys. Chem. A* **2006**, *110*, 7593−7601.
(35) Burden, D. K.; Johnson, A. M.; Nathanson, G. M. HCl Uptake through Films of Pentanoic Acid and Pentanoic Acid/Hexanol Mixtures at the Surface of Sulfuric Acid. *J. Phys. Chem. A* **2009**, *113*, 14131−14140.
(36) Park, S.-C.; Burden, D. K.; Nathanson, G. M. Surfactant Control of Gas Transport and Reactions at the Surface of Sulfuric Acid. *Acc. Chem. Res.* **2009**, *42*, 379−387.
(37) Williams, L. R.; Long, F. S. Viscosity of Supercooled Sulfuric Acid Solutions. *J. Phys. Chem.* **1995**, *99*, 3748−3751.
(38) Carslaw, K. S.; Clegg, S. L.; Brimblecombe, P. A Thermodynamic Model of the System $HCl-HNO_3-H_2SO_4-H_2O$, Including Solubilities of HBr, from <200 to 328 K. *J. Phys. Chem.* **1995**, *99*, 11557−11574. Wexler, A. S.; Clegg, S. L. Atmospheric Aerosol Models for Systems Including the ions H^+, NH_4^+, Na^+, SO_4^{2-}, NO_3^-, Cl^-, Br^-, and H_2O. *J. Geophys. Res.* **2002**, *107*, D14−4207 Calculations from the aerosol inorganics model at http://www.aim.env.uea.ac.uk/aim/aim.php..
(39) Myhre, C. E. L.; Christensen, D. H.; Nicolaisen, F. M.; Nielsen, C. J. Spectroscopic Study of Aqueous H_2SO_4 at Different Temperatures and Compositions: Variations in Dissociation and Optical Properties. *J. Phys. Chem. A* **2003**, *107*, 1979−1991.
(40) Que, H.; Song, Y.; Chen, C.-C. Thermodynamic Modeling of the Sulfuric Acid−Water−Sulfur Trioxide System with the Symmetric Electrolyte NRTL Model. *J. Chem. Eng. Data* **2013**, *56*, 963−977.
(41) Margarella, A. M.; Perrine, K. A.; Lewis, T.; Faubel, M.; Winter, B.; Hemminger, J. C. Dissociation of Sulfuric Acid in Aqueous Solution: Determination of the Photoelectron Spectral Fingerprints of H_2SO_4, HSO_4^-, and SO_4^{2-} in Water. *J. Phys. Chem. C* **2013**, *117*, 8131−8137.

(42) Iraci, L. T.; Essin, A. M.; Golden, D. M. Solubility of Methanol in Low-Temperature Aqueous Sulfuric Acid and Implications for Atmospheric Particle Composition. *J. Phys. Chem. A* **2002**, *106*, 4054−4060.
(43) Lee, D. G.; Cameron, R. The Basicity of Ethanol. An Acidity Function for Alcohols. *J. Am. Chem. Soc.* **1971**, *93*, 4724−4728.
(44) *ACD/ChemSketch Freeware*, version 12.01; Advanced Chemistry Development, Inc.: Toronto, ON, Canada, 2009; http://www.acdlabs.com.
(45) Can, S. Z.; Mago, D. D.; Walker, R. A. Structure and Organization of Hexadecanol Isomers Adsorbed to the Air/Water Interface. *Langmuir* **2006**, *22*, 8043−8049.
(46) Henry, D. J.; Dewan, V. I.; Prime, E. L.; Qiao, G. G.; Solomon, D. H.; Yarovsky, I. Monolayer Structure and Evaporation Resistance: A Molecular Dynamics Study of Octadecanol on Water. *J. Phys. Chem. B* **2010**, *114*, 3869−3878.
(47) Lawrence, J. R.; Glass, S. V.; Nathanson, G. M. Evaporation of Water through Butanol Films at the Surface of Supercooled Sulfuric Acid. *J. Phys. Chem. A* **2005**, *109*, 7449−7457.
(48) We verified that steady surface concentrations were reached for the BuOD, HexOD, and EtBuOD films by spinning the coated wheel at twice the speed and measuring nearly identical scattering patterns; the average deviations in the fractional Argon energy transfer and H→D exchange fractions were each less than 0.01.
(49) Butt, H.-J.; Graf, K.; Kappl, M. *Physics and Chemistry of Interfaces*, 3rd ed.; Wiley-VCH: Weinheim, Germany, 2013; Chapter 8.
(50) Defay, R.; Prigogine, I. *Surface Tension and Adsorption*; Wiley: New York, 1966; Chapters 2 and 7.
(51) Torn, R. D.; Nathanson, G. M. Surface Tensions and Surface Segregation of n-Butanol in Sulfuric Acid. *J. Phys. Chem. B* **2002**, *106*, 8064−8069.
(52) Van Loon, L. L.; Minor, R. N.; Allen, H. C. Structure of Butanol and Hexanol at Aqueous, Ammonium Bisulfate, and Sulfuric Acid Solution Surfaces Investigated by Vibrational Sum Frequency Generation Spectroscopy. *J. Phys. Chem. A* **2007**, *111*, 7338−7346.
(53) Chen, B.; Siepmann, J. I.; Klein, M. L. Vapor−Liquid Interfacial Properties of Mutually Saturated Water/1-Butanol Solutions. *J. Am. Chem. Soc.* **2002**, *124*, 12232−12237.
(54) Krisch, M. J.; D'Auria, R.; Brown, M. A.; Tobias, D. J.; Hemminger, J. C.; Ammann, M.; Starr, D. E.; Bluhm, H. The Effect of an Organic Surfactant on the Liquid−Vapor Interface of an Electrolyte Solution. *J. Phys. Chem. C* **2007**, *111*, 13497−13509.
(55) Sakaguchi, S.; Morita, A. Molecular Dynamics Study of Water Transfer at Supercooled Sulfuric Acid Solution Surface Covered with Butanol. *J. Phys. Chem. A* **2013**, *117*, 4602−4610.
(56) Yan, T. Y.; Isa, N.; Gibson, K. D.; Sibener, S. J.; Hase, W. L. Role of Surface Intramolecular Dynamics in the Efficiency of Energy Transfer in Ne Atom Collisions with a n-Hexylthiolate Self-Assembled Monolayer. *J. Phys. Chem. A* **2003**, *107*, 10600−10607.
(57) Day, B. S.; Morris, J. R. Packing Density and Structure Effects on Energy-Transfer Dynamics in Argon Collisions with Organic Monolayers. *J. Chem. Phys.* **2005**, *122*, 234714.
(58) Rettner, C. T.; Schweizer, E. K.; Mullins, C. B. Desorption and Trapping of Argon at a 2H-W(100) Surface as a Test of the Applicability of Detailed Balance to a Nonequilibrium System. *J. Chem. Phys.* **1989**, *90*, 3800−3813.
(59) Morris, J. R.; Behr, P.; Antman, M. D.; Ringeisen, B. R.; Splan, J.; Nathanson, G. M. Molecular Beam Scattering from Supercooled Sulfuric Acid: Collisions of HCl, HBr, and HNO_3 with 70 wt % D_2SO_4. *J. Phys. Chem. A* **2000**, *104*, 6738−6751.
(60) Gilde, A.; Siladke, N.; Lawrence, C. P. Molecular Dynamics Simulations of Water Transport through Butanol Films. *J. Phys. Chem. A* **2009**, *113*, 8586−8590.
(61) Nathanson, G. M. Molecular Beam Studies of Gas−Liquid Interfaces. *Annu. Rev. Phys. Chem.* **2004**, *55*, 231−255.
(62) Klassen, J. K.; Hu, Z. J.; Williams, L. R. Diffusion Coefficients for HCl and HBr in 30 to 72 wt % Sulfuric Acid at Temperatures between 220 and 300 K. *J. Geophys. Res. Atmos.* **1998**, *103*, 16197−16202.
(63) Ardura, D.; Donaldson, D. J. Where Does Acid Hydrolysis Take Place? *Phys. Chem. Chem. Phys.* **2009**, *11*, 857−863.
(64) Wick, C. D. HCl Accommodation, Dissociation, and Propensity for the Surface of Water. *J. Phys. Chem. A* **2013**, *117*, 12459−12467.
(65) Uras-Aytemiz, N.; Devlin, J. P.; Saldlej, J.; Buch, V. HCl Solvation at the Surface and within Methanol Clusters/Nanoparticles II: Evidence for Molecular Wires. *J. Phys. Chem. B* **2006**, *110*, 21751−21763.
(66) Chorny, I.; Benjamin, I.; Nathanson, G. M. Scattering, Trapping, and Ionization of HCl at the Surface of Liquid Glycerol. *J. Phys. Chem. B* **2004**, *108*, 995−1002.
(67) Behr, P.; Morris, J. R.; Antman, M. D.; Ringeisen, B. R.; Splan, J. R.; Nathanson, G. M. Reaction and Desorption of HCl and HBr Following Collisions with Supercooled Sulfuric Acid. *Geophys. Res. Lett.* **2001**, *28*, 1961−1964.
(68) Luck, W. A. P.; Schrems, O. Infrared Spectroscopic Studies on Hydrogen Chloride Alcohol Complexes. *Chem. Phys. Lett.* **1980**, *76*, 75−79.
(69) Lee, D. G.; Demchuk, K. J. A Carbon 13 Nuclear Magnetic Resonance Study of the Basicities of Aliphatic Alcohols. *Can. J. Chem.* **1987**, *65*, 1769−1774.
(70) We note that the analysis of HCl uptake through pentanoic acid films also yielded comparable blocking parameters of 1.3 and 1.1 for 60 and 68 wt % D_2SO_4. Like EtBuOH, these films also reduced HCl entry below the bare acid values. See ref 35.